Journal of Zhejiang University-SCIENCE A (Applied Physics & Engineering)
ISSN 1673-565X (Print); ISSN 1862-1775 (Online)
www.jzus.zju.edu.cn; www.springerlink.com
E-mail: jzus@zju.edu.cn

Effect of hygrothermal environment on the tension–tension fatigue performance and reliable fatigue life of T700/MTM46 composite laminates*

Bin-lin MA, Yu FENG†‡, Yu-ting HE, Teng ZHANG, Sheng ZHANG, Tian-yu ZHANG

Aeronautics Engineering College, Air Force Engineering University, Xi'an 710038, China

†E-mail: fynuaa@126.com

Received Mar. 4, 2019; Revision accepted May 19, 2019; Crosschecked June 6, 2019

Abstract: The tension–tension fatigue performance of T700/MTM46 composite laminates after hygrothermal aging was investigated and compared with those of virgin T700/MTM46 laminates. The most significant failure mode of the moisture-saturated fatigue specimens is still severe delamination, and the stiffness degradation of moisture-saturated fatigue specimens can be divided into two distinct stages. However, the hygrothermal conditions will aggravate the stiffness degradation of the composite laminates during fatigue. Damage evolution was studied by the edge view of the specimens. The degree of damage of the saturated specimens is more serious than that of the virgin specimens at the same percentage of fatigue life during the fatigue process, especially in the initial stage. The distribution of fatigue life in each stress level was determined. The *p*-*γ*-*S*-*N* surfaces were established to predict a reliable fatigue life. The results show that the reliable fatigue life of the moisture-saturated specimens is much lower than that of the virgin specimens under the same conditions. Although the hygrothermal environment does not show a significant effect on the static tensile properties of the T700/MTM46 composite laminates, the fatigue performance is significantly degenerated.

Key words: Carbon fiber reinforced polymer; Hygrothermal conditions; Fatigue performance; Damage evolution; *p*-*γ*-*S*-*N* surfaces

https://doi.org/10.1631/jzus.A1900081 **CLC number:** V25

1 Introduction

The high specific strength and specific stiffness of composite materials, especially fiber reinforced polymer (FRP) composites, make them suitable for use in the aerospace industry (Riccio, 2015). A higher proportion of advanced composite materials is used each year in the construction of each new generation of aerospace structures (Maria, 2013). Previous investigators have studied the mechanical performance of FRP composites (Yao and Himmel, 1999; van Paepegem and Degrieck, 2002; Hosoi et al., 2006; Degenhardt et al., 2008; Zafar et al., 2012; Riccio et al., 2014; Khechen, 2015; Mallela and Upadhyay, 2016; Feng et al., 2017b; Arani and Zamani, 2018; Caminero et al., 2018; Montesano et al., 2018). As an advanced aerospace material, carbon fiber reinforced polymer (CFRP) composites are widely applied in aeronautics engineering for primary load-bearing structures and parts (Montesano et al., 2013). Compared with traditional metal or alloy materials, CFRP composites possess higher specific strength and stiffness, and better resistance to corrosion and fatigue, and thus can make the aircraft lighter and

‡ Corresponding author

* Project supported by the National Natural Science Foundation of China (No. 51805538) and the Young Talent Fund of University Association for Science and Technology in Shaanxi Province, China (No. 20190410)

ORCID: Bin-lin MA, https://orcid.org/0000-0001-6749-9617; Yu FENG, https://orcid.org/0000-0002-4634-9465

improve its performance (Mohaghegh, 2018). They are now replacing conventional aeronautic aluminum and titanium alloys (Maria, 2013).

A cyclic fatigue load is the primary load on the internal components during aircraft service. Although CFRP composites have good fatigue resistance, research into the fatigue performance of CFRP composites has been carried out (Yao and Himmel, 1999; Hosoi et al., 2006; Montesano et al., 2012; Feng et al., 2017a, 2017c) because of their long service life in aircraft (usually more than 30 years). Yao and Himmel (1999) proposed a method for estimating the residual strength of polymer composites based on data from truncated fatigue life experiments. This analysis method showed a high fitting accuracy with the experimental data. Hosoi et al. (2006) investigated the fatigue behavior of quasi-anisotropic CFRP composite laminates under a loading sequence of variable amplitude. The cumulative damage was evaluated by using residual strength as a parameter, and the internal micro-damage was observed by optical microscope. Montesano et al. (2012) studied the fatigue behavior and damage mechanism of a woven-fabric CFRP laminate under on-axial and off-axial tensile cyclic loading. It was observed from experimental results that fatigue properties between the on-axis and off-axis samples vary, evidently because of anisotropic damage development. Substantive studies (van Paepegem and Degrieck, 2002; Manjunatha et al., 2010; Peng et al., 2015; Zhao et al., 2016) have shown that composites exhibit significant degradation in stiffness during the fatigue process. Tate and Kelkar (2008) studied the stiffness degradation of bi-directional braided carbon fiber/epoxy resin matrix composites with different braiding angles under a tension–tension fatigue load. Duan and Yao (2002) suggested a prediction model for stiffness degradation induced by matrix cracking for FRP laminates under in-plane tension. The scattering of fatigue life data of CFRP composites which exhibit many failure modes, is greater than that of metals or alloys. Feng et al. (2016) studied the reliability tension–tension fatigue life of T700/MTM46 composites. The results showed that their fatigue life obeys a lognormal distribution and a new fatigue model predicting the reliable fatigue life was established.

However, CFRP composites are sensitive to some factors (Mallela and Upadhyay, 2006), such as low velocity impact (Riccio et al., 2013; Feng et al., 2017b), hygrothermal environment (Zafar et al., 2012; Feng et al., 2015; Tual et al., 2015), and imperfections (Degenhardt et al., 2014), which restrict the further application of CFRP composite materials in aircraft. Among them, the hygrothermal environment has a great influence on the performance of the CFRP composites commonly used in aircraft, and is increasingly of concern to aircraft designers. The word "hygrothermal" describes the combined effects of moisture and temperature on composites.

The influence of the hygrothermal environment on composites is complex, including many chemical and physical changes. Increased temperature causes a softening of CFRP composites, and a corresponding degradation of performance (Gibson, 2016). However, García-Moreno et al. (2019a, 2019b) found that before the operating temperature is lower than the glass transition temperature (T_g), the short period of temperature aging will lead to a post-curing process, which can enhance the fiber matrix interface. Moisture absorption causes the reduction of T_g because of the plasticization of materials, and the consequent degradation of the properties of composites (Gibson, 2016). On the other hand, hygrothermal expansions alter the stress distribution, and thus affect the mechanical properties of the composites (Gibson, 2016). The changes in mechanical properties of composites after hydrothermal aging are thus very complicated. Tual et al. (2015) reported that the tensile strength of CFRP specimens decreased significantly while the tensile modulus remained almost unchanged after hydrothermal aging. Joshi (1983) investigated the tensile strength degradation of ±45° CFRP laminates under the hygrothermal environment, and showed that the tensile strength decreases from 220 MPa to 140 MPa when the temperature is raised from 20 °C to 130 °C. Patel and Case (2000) studied the effect of hygrothermal environment on the durability of graphite/epoxy resin composites; the fatigue life was predicted based on residual strength. These results indicated that the strength and modulus of aged specimens decreased slightly compared with those of a virgin specimen. Adda-Bedia et al. (2008) established a shear hysteresis model considering the radial modulus change caused by transverse cracks, to predict the stiffness degradation of symmetric laminates [0m/90n] after aging in a hygrothermal environment.

Kootsookos and Mouritz (2004) performed 4-point bending work on polyester and vinyl ester CFPR, and showed that, whereas the strength does deteriorate, the variation of flexural modulus has no statistical significance. Sun et al. (2011) assessed the effect of hygrothermal conditions on the interlaminar shear strength of CFRP at 23–150 °C. Their experimental results showed that the interlaminar shear performance decreases with the increase in moisture absorption time, and stabilizes at about 14 d, which was independent of temperature. Feng et al. (2010) elucidated the importance of moisture content on the interlaminar shear properties of CFRP. The degradation degree of the interlaminar shear strength is basically the same, when the same moisture content is achieved under different hygrothermal conditions.

Existing research has mainly focused on the effect of hygrothermal aging on the static strength of composites by using both experimental and numerical methods. However, there is less research on the effect of the hygrothermal environment on the reliable fatigue life. Fatigue performance has a great influence on the safety and reliability of composites, and the hygrothermal environment has itself a great influence on it. It is necessary, therefore, to study further the effects of hygrothermal aging on the fatigue performance of composite materials. In this paper, the tension–tension fatigue test of T700/MTM46 composite laminates under hygrothermal environment is described, and the tension–tension fatigue performance and reliable fatigue life of T700/MTM46 composite laminates after hygrothermal aging are discussed. The results are compared with those under normal conditions (Feng et al., 2016), and the effects of hygrothermal environment on tension–tension fatigue performance and reliable fatigue life of T700/MTM46 composite laminates are clarified.

2 Experimental

2.1 Preparation of specimens

A carbon/epoxy composite laminate with 2 mm thickness glass/polymer end-tabs was designed according to ASTM D3039/D3039M (ASTM, 2007) and ASTM D3479/D3479M (ASTM, 2012) (Fig. 1). Specimens were manufactured by using carbon fiber/epoxy resin T700/MTM46 prepreg provided by AVIC Beijing Institute of Aeronautics Materials, China.

The materials were cured in an autoclave facility using a two-step cure cycle. The temperature was first increased to 70 °C for 1.5 h, and then was increased to 135 °C and held for 1 h. Mechanical properties of the materials are listed in Table 1. The stacking sequence of the specimens is [45/90/−45/0/45/0/−45/90/0]s. The nominal dimensions of specimens and end-tabs were 250 mm×25 mm×2.4 mm and 55 mm×25 mm×2 mm, respectively.

The end-tabs at both ends of the specimens were made of GFRP, and they also absorb moisture from the hygrothermal environment. If moisture content measuring is achieved by directly weighing the specimens, the moisture absorption of the end-tabs will be included, which may result in inaccurate moisture content data. Therefore, three moisture absorption specimens (Fig. 2) were used to measure the moisture content, and the material and lay-up of these were exactly the same as those of the above fatigue specimens.

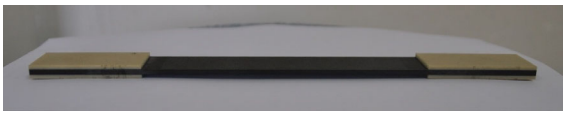

Fig. 1 Geometric shape of fatigue specimens

Table 1 Material properties

E_{11} (MPa)	E_{22} (MPa)	E_{33} (MPa)	G_{12} (MPa)	G_{13} (MPa)	G_{23} (MPa)	υ_{12}	υ_{13}	υ_{23}
124 130	8800	8800	4470	4470	3260	0.33	0.45	0.33

E_{11}, E_{22}, E_{33} are Young's moduli along the 1, 2, and 3 directions; G_{12}, G_{13}, G_{23} are shear moduli associated with the 12, 13, and 23 planes; υ_{12}, υ_{13}, υ_{23} are Poisson's ratios

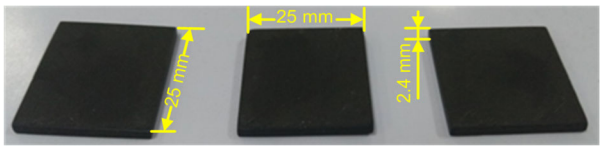

Fig. 2 Geometric shape of moisture absorption specimens

2.2 Experimental procedure

According to ASTM D5229/D5229M (ASTM, 2004), the condition for the moisture absorption experiment was a water bath at 70 °C, and the tests

were carried out in a hygrothermal environment box with a precision of 0.1 °C. Before the moisture absorption experiment, the moisture absorption specimens and fatigue specimens were put together in a drying oven at 70 °C for drying treatment. The weight of specimens was measured at 24-h intervals by an electronic balance with a precision of 0.001 g. When the mass decrement or increment of the moisture absorption specimens was less than 0.01% in three consecutive measuring cycles, all the specimens were considered to have reached either an engineering dry state or effective moisture equilibrium.

The test conditions for the static tension and tension–tension fatigue tests were the same as those in (Feng et al., 2016), and Fig. 3 shows the mechanical experimental setups. Static tests of three specimens were carried out to determine their ultimate tensile strength (UTS) on an MTS-810 servo-hydraulic test machine (MTS Systems Corporation, USA). The static test was conducted under displacement control mode at a displacement rate of 1 mm/min until the final failure occurred. The strain in the tensile direction of the specimen was measured by an extensometer with a 50-mm gauge length. Fatigue tests of the specimens were conducted with the MTS-810 in load control mode using a sinusoidal wave form at a frequency of 10 Hz and a stress ratio R=0.1. The ratios of stress to UTS (normalized stress q) used were 0.90, 0.85, 0.80, 0.75, 0.70, and 0.65. The fatigue experimental procedure stopped when the specimens failed or the fatigue life reached 1×10^6 cycles (Giancane et al., 2010).

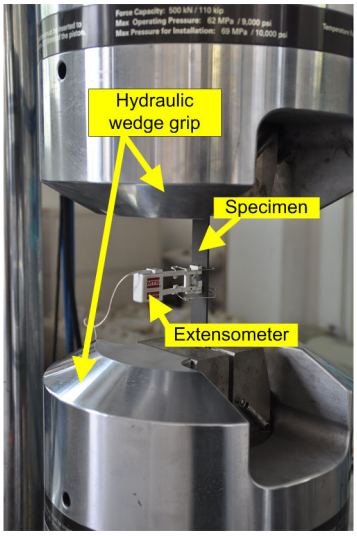

Fig. 3 Experimental setups

3 Results and discussion

3.1 Moisture absorption experiment

The initial masses of the three moisture absorption specimens were 2.811 g, 2.657 g, and 2.671 g. The three moisture absorption specimens reached moisture equilibrium with 1.67%, 1.84%, and 1.57% moisture contents after 43 measuring cycles (1#, 2#, and 3# in Fig. 4, respectively). It can be seen from Fig. 4 that the moisture content as a function of immersion time increased rapidly in the early stage of moisture absorption, and then increased gradually and plateaued at approximately 40 d indicating a two-stage diffusion response. The first stage, occurring at a rapid rate, is considered to be a Fickian response, while the second stage is less rapid and is due to a combination of filling of pores and wicking. A similar phenomenon was also observed by Bao and Yee (2002) and Karbhari and Xian (2009).

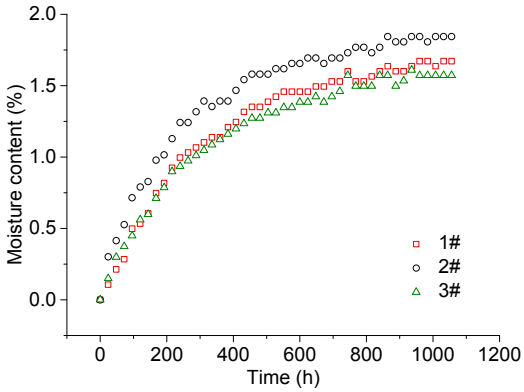

Fig. 4 Moisture absorption curves of the specimens

Specimens were taken out from the environmental box at a certain time, and the edge views of these specimens were examined by an optical microscope (30×) to investigate the damage of the specimens during moisture absorption, as shown in Fig. 5. Before moisture absorption (Fig. 5a), the interlaminar bonding is very tight, and there are no cracks, delamination, or other damage. It is shown that some micropores appear in the ±45° and 90° plies, caused by the looseness of the matrix within the plies, as seen in Fig. 5b. In Fig. 5c, in addition to the obvious increase of micropores, there are some slight delaminations, including inter-ply and intra-ply delaminations. However, the delamination degree is

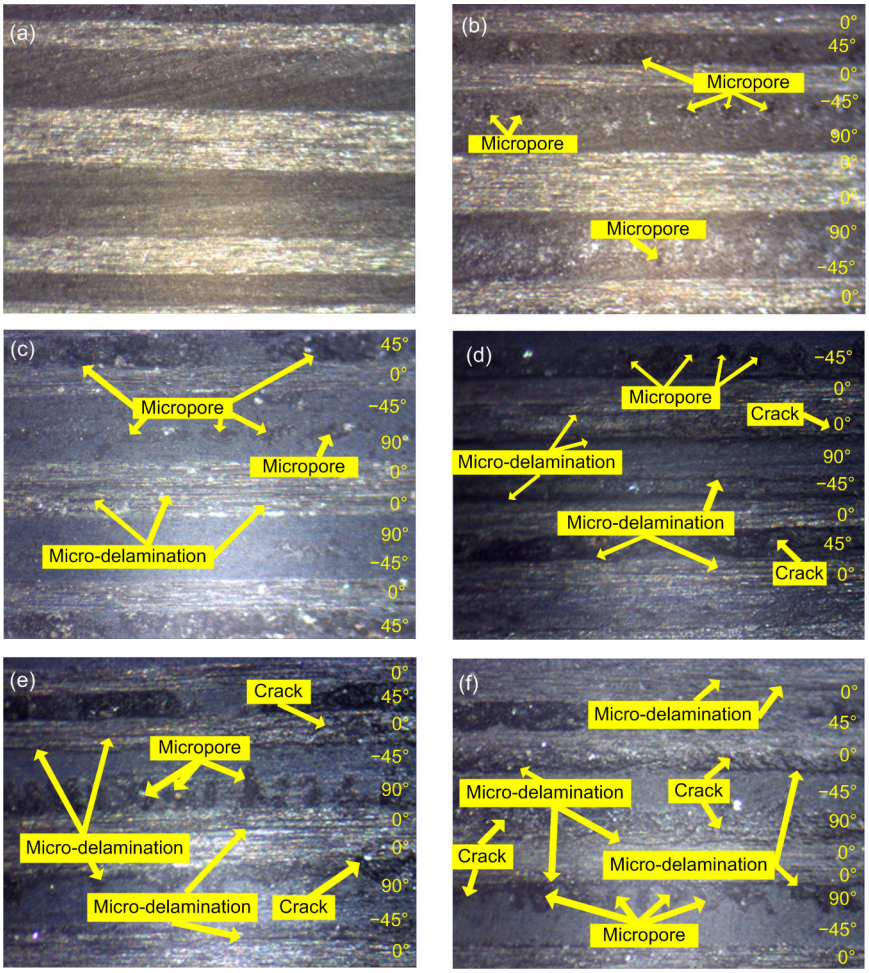

Fig. 5 Damage evolution of fatigue specimen during moisture absorption at: (a) 0 d; (b) 5 d; (c) 10 d; (d) 20 d; (e) 30 d; (f) 40 d

obviously weaker than that in the fatigue process (Feng et al., 2016). In Fig. 5d, it can be seen that the damage has grown significantly, the micropores have increased further, and some plies have slight intra-ply and inter-ply delaminations. In addition, some plies other than 0° plies also show a few cracks. Damage has grown slightly at the 30th and 40th days (as shown in Figs. 5e and 5f, respectively), compared with those observed at the 20th day (Fig. 5d) during moisture absorption. Therefore, the damage growth of T700/MTM46 CFRP laminates in hygrothermal environment can be divided into two stages: a rapid damage growth stage during the first 20 d and a slower damage growth stage after the 20th day. At the same time, the moisture absorption curve (Fig. 4) can also be divided into two stages, including the early rapid stage and the later slow stage, and the critical value between the two stages is also about 20 d. Therefore, it can be inferred that the early rapid moisture absorption stage is not only caused by initial cracks and pores, but also the micropores; cracks and micro-delamination damage generated in moisture absorption will further accelerate the moisture absorption rate in this stage. In the later stage, the growth rate of these damages is slower, which further increases the difference in moisture absorption rates between the two stages.

3.2 Static tension experiment

The static experimental results of the three moisture-saturated specimens are listed in Table 2. The variation coefficients C_v (the standard deviation/average value ratio, representing the scattering of data) of UTS, moduli, and ultimate strain are 1.417%, 1.861%, and 3.308%, respectively, indicating the experimental results are less dispersive. In Table 2,

Table 2 Comparison of static experimental results under different conditions

Condition		UTS (MPa)	Young's modulus, E (GPa)	Ultimate strain
Hygrothermal	Specimen No. 1	842.9	51.1	0.016 50
	Specimen No. 2	825.1	48.6	0.016 98
	Specimen No. 3	820.7	48.0	0.017 09
	Average	829.567	49.233	0.016 86
Normal (Feng et al., 2016)	Average	840.633	49.233	0.017 07
Average decrement		1.3%	0.0%	1.2%

the mean values of the static experimental results of the moisture-saturated specimens are compared with the data of virgin specimens (Feng et al., 2016), and the UTS and ultimate strain decreases by 1.3% and 1.2%, respectively, while Young's moduli basically remain unchanged. However, considering the scattering of the material itself, the UTS and ultimate strain have not in fact changed significantly. Therefore, it can be concluded that the hygrothermal environment does not have a significant effect on the static tensile properties of T700/MTM46 laminates. The static tensile properties are mainly controlled by fibers, while the hygrothermal environment generally has a greater influence on the matrix and fiber-matrix interface properties, and has less influence on the fibers (Zhang et al., 2012), so there is no significant decrease in the static experimental data of moisture-saturated specimens compared with that for virgin specimens.

For the virgin specimens, the failure mode is mainly brittle fracture in a small area near the middle of the specimen, and there is no obvious delamination phenomenon (Feng et al., 2016). Although the UTS and Young's modulus of saturated specimens do not change significantly after hygrothermal treatment, the static failure modes of saturated specimens are slightly different from those of virgin specimens in (Feng et al., 2016), as shown in Fig. 6. The failure of saturated specimens tends to appear as multiple fractures throughout the gauge length while the brittle facture is dominant for virgin specimens with a small fracture region. In addition to fracture and pulling out of the fiber bundles and matrix fragments, the failure modes also include a certain degree of delamination which is more obvious than the delamination degree of virgin specimens during the static tests in (Feng et al., 2016). The reason for delamination is that some micro-delaminations are formed in the process of moisture absorption and have grown to a certain extent under the static load.

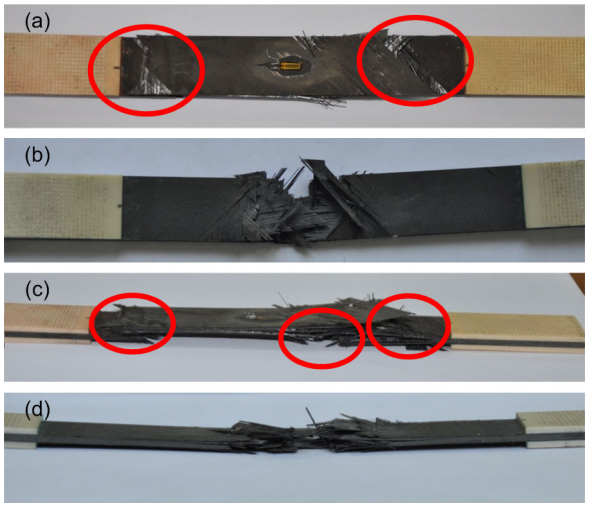

Fig. 6 Static failure modes of saturated specimen (a) and virgin specimen (b) from top view, and saturated specimen (c) and virgin specimen (d) from edge view

3.3 Tension–tension fatigue experiment

The tension–tension fatigue life of fatigue specimens at various stress levels is shown in Table 3, and the value with arrow represents the fatigue life over 1×10^6 cycles. The variation coefficients C_v of the fatigue life of the specimens at each stress level are shown in Table 4. It can be seen that under the same normalized stress level, the fatigue life variation coefficients of the saturated specimens are larger than those of the virgin specimens, which indicates that the fatigue life scattering of the CFRP laminates is increased after hygrothermal treatment. The reason for this phenomenon is the inhomogeneity in the processing of composite materials. It is well known that composites have inhomogeneous properties (Amara et al., 2005) because of the inhomogeneity of defects.

In addition, the micropores and micro-delaminations of specimens generated during the moisture absorption process are also randomly distributed. Although the specimens as whole components, have achieved moisture absorption saturation, the local moisture contents are different in each micro region with different porosities, which leads to different degrees of physical and chemical changes. Therefore, the inhomogeneity of the moisture-saturated specimens is further increased, which results in the variation in fatigue life of the saturated specimens being larger than that of the virgin specimens.

Table 3 Fatigue life data at various stress levels

No.	Fatigue life (cycles)					
	q=0.90	q=0.85	q=0.80	q=0.75	q=0.70	q=0.65
1	1886	3017	52 541	126 876	218 521	684 795
2	557	17 490	20 842	445 862	621 334	774 689
3	834	27 002	169 852	319 206	695 212	514 121
4	1332	6544	14 816	284 587	432 453	1 000 000 →
5	188	6453	113 252	720 812	298 521	916 547

Table 4 Variation coefficients of fatigue life data at various stress levels

Condition	Variation coefficient (%)					
	q=0.65	q=0.70	q=0.75	q=0.80	q=0.85	q=0.90
Hygrothermal	24.6	45.2	58.5	89.1	82.3	69.3
Normal (Feng et al., 2016)	–	35.8	54.5	78.3	71.7	54.0

The *S*-*N* curves of the saturated and virgin specimens are shown in Fig. 7. A classical exponent law representation (Gao et al., 2013) of the *S*-*N* curve is also adopted to plot the *S*-*N* curve of specimens, and the form of the *S*-*N* equation is:

$$S = \lg C / (m \lg \mathrm{e}) + 1 / (m \lg \mathrm{e} \cdot \lg N), \tag{1}$$

where S is the normalized stress level, N is the fatigue cycles to failure, which represents the fatigue life. m and C are material constants. For moisture-saturated specimens, the expression of the *S*-*N* curve is y=1.115–0.071x, where x and y are the log-fatigue life and normalized maximum stress, respectively. In Fig. 7, it is obvious that the *S*-*N* curve of the moisture-saturated specimens is entirely below that of the virgin specimens, which means that the fatigue life of the saturated specimens is lower than that of the virgin specimens at the same stress level. According to the *S*-*N* curve, the fatigue limit under which the specimens can survive after being subjected to 1×10^6 cycles, is about 0.654, or 542.54 MPa for T700/MTM46 saturated specimens, which is approximately 6% lower than that for virgin specimens (0.686, 576.67 MPa) in (Feng et al., 2016).

According to Feng et al. (2016), and assuming that the fatigue life of the specimens in this study obeys log-normal distribution and the median fatigue life is selected to quantitatively illustrate the degree of decline in the fatigue life of the T700/MTM46 laminates after hygrothermal aging at each stress level, the median fatigue lives of the T700/MTM46 laminates at stress levels of 0.90, 0.85, 0.80, 0.75, and 0.70 decrease by 40.3%, 37.2%, 34.3%, 23.1%, and 42.5%, respectively, after hygrothermal aging. The median fatigue life decreases obviously after the hygrothermal treatment.

The degree of damage in composites can be evaluated by measuring stiffness degradation, E_N/E_1, which can be calculated by (Judawisastra et al., 1998)

$$\frac{E_N}{E_1} = \frac{\left(\dfrac{\Delta p}{\Delta d}\right)_1 - \left(\dfrac{\Delta p}{\Delta d}\right)_N}{\left(\dfrac{\Delta p}{\Delta d}\right)_1}, \tag{2}$$

where E_N and E_1 represent Young's moduli of the material measured at the given cycle and the first cycle, respectively. Δp is the difference between maximum and minimum loads, and Δd is the corresponding displacement of the specimen. In the stiffness degradation curve, the normalized fatigue life is plotted versus the normalized stiffness, as shown in Fig. 8. The lines with S and V represent the stiffness degradation curves of saturated specimens in this study and the virgin specimens in (Feng et al., 2016), respectively.

In Fig. 8, it can be seen that the stiffness decreases most at q=0.65 and least at q=0.90. With the decrease of stress level, the stiffness decreases gradually, which is consistent with that of virgin specimens in (Feng et al., 2016). The trends of the normalized stiffness degradation curves of the saturated specimens and the virgin specimens are similar and

can be divided into two stages. The stiffness decreases at a quasi-constant slow rate during approximately 0–83% of the fatigue life N_f in the first stage, while after around the 83% fatigue life the stiffness shows a relatively large decreasing trend in the second stage. These characteristics are very similar to those of virgin specimens in (Feng et al., 2016). In addition, it can be seen from Fig. 8 that the stiffness of specimens after the hygrothermal treatment is more severely degraded under the same fatigue life percentage. The ultimate stiffness degradation of specimens increases by 15.7%, 4.6%, 11.6%, 13.4%, and 13.2% after the hygrothermal treatment under 0.70, 0.75, 0.80, 0.85, and 0.90 stress levels, respectively. In conclusion, the hygrothermal conditions will aggravate the stiffness degradation of the composite laminates during fatigue.

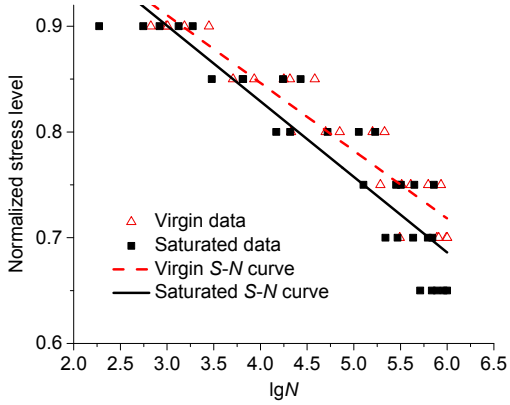

Fig. 7 *S-N* curves of saturated and virgin laminates

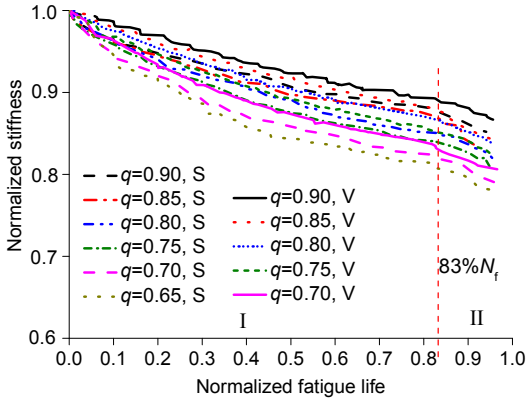

Fig. 8 Stiffness degradation curves of normalized fatigue life

The No. 1 fatigue specimen under q=0.80 stress level (N_f=52 541 cycles) was selected as the representative to describe the fatigue damage evolution of the moisture-saturated specimens. Edge views of it during the fatigue experiment were observed by optical microscope (30×), as shown in Fig. 9. According to the analysis of Section 3, some micro-damage has been produced in specimens during the moisture absorption process before the fatigue test. Therefore, compared with the virgin specimens in (Feng et al., 2016), the moisture-saturated specimens have slight damage before the fatigue test. When the fatigue cycles reach N_a=400 cycles (about 0.76%N_f, Fig. 9a), many damage modes, such as inter-ply delamination, intra-ply delamination, matrix cracks, and some separated fiber bundles, appear in each ply. The damage began to initiate and develop from the beginning of the fatigue cycling. However, there was only a low degree of intra-ply delamination in 90° plies at 500 cycles (about 0.71%N_f) for virgin specimens in (Feng et al., 2016). Although the damage of the moisture-saturated and the virgin specimens is generated from the initial stage of the fatigue process, the damage degree of the saturated specimens is much greater than that of the virgin specimens in the initial stage. The reason for this phenomenon is that the specimens have been damaged during the moisture absorption process. Although the damage is marginal, it can develop more rapidly under fatigue loading and also lead to further new damage. When the fatigue cycles reach N_b=4000 cycles (about 7.61%N_f, Fig. 9b), the pulled-out fibers in 0° plies besides the damage modes at 400 cycles are observed. A far greater amount of transverse and oblique cracks, inter/intra-ply delaminations, and separated fiber bundles can be found, and the degree of damage is further aggravated. In Fig. 9c (N_c=45 000 cycles, about 85.65%N_f), in addition to the aforementioned damage modes, a large number of fiber breakages in 0° plies appear before the ultimate catastrophic failure of specimens during fatigue, this is a damage mode not found at 400 and 4000 cycles. In addition, it is noted that the rapid reduction in stiffness of specimens before fatigue failure was basically during the 83%–85% fatigue life in Fig. 8. As a consequence, the fiber breakage in the 0° plies may contribute to the rapid decline of stiffness in the later stage of the fatigue process, thus leading to a catastrophic failure. This conclusion is consistent with the corresponding conclusion for the T700/MTM46 virgin specimens in (Feng et al., 2016).

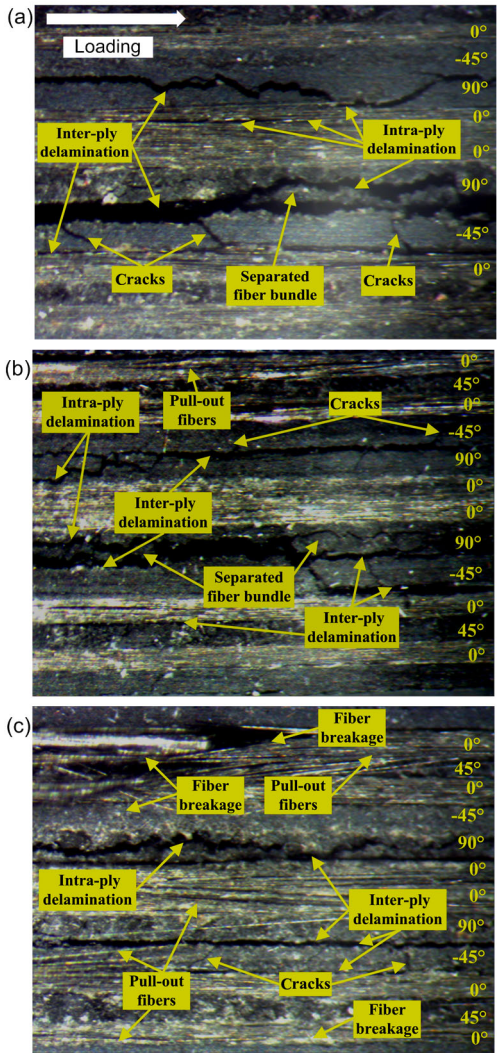

Fig. 9 Edge views of moisture-saturated fatigue specimen under q=0.8 stress level at 400 cycles (a), 4000 cycles (b), and 45 000 cycles (c)

The fatigue failure modes of saturated specimens at each stress level and virgin specimen at q=0.85 stress level from the top/edge view are shown in Fig. 10. It can be seen that the fatigue failure modes of the specimens include delamination, fiber pull-out, fiber breakage, and so on, but the most significant failure mode is still severe delamination, which is very similar to the fatigue failure modes of the virgin specimens in (Feng et al., 2016). From visual observation, it is difficult to identify the difference of degree of delamination between fatigue specimens at different stress levels, and the delamination degree does not show obvious regularity with the change of stress level. Moreover, the delamination of the virgin specimens after fatigue failure was also severe in (Feng et al., 2016), so it seems that the delamination degree of the moisture-saturated specimens in this study is not significantly higher than that of the virgin specimens in (Feng et al., 2016) after fatigue failure at the corresponding stress level.

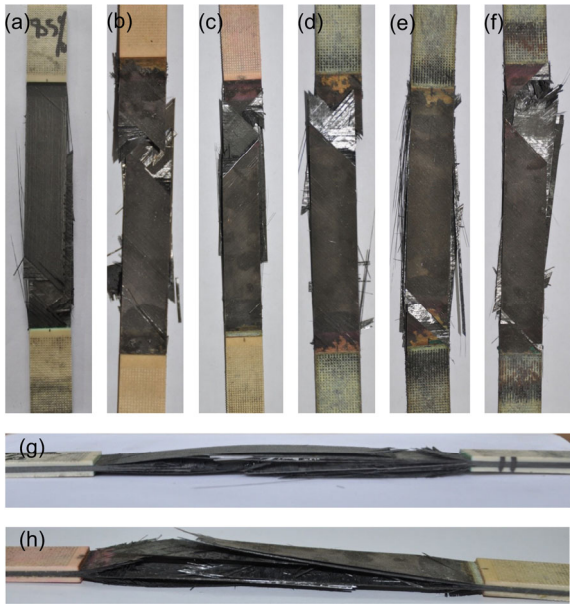

Fig. 10 Fatigue failure modes of virgin specimen (q=0.85) (a), saturated specimen (q=0.90) (b), saturated specimen (q=0.85) (c), saturated specimen (q=0.80) (d), saturated specimen (q=0.75) (e), and saturated specimen (q=0.70) (f) from top view, and virgin specimen (q=0.85) (g) and saturated specimen (q=0.85) (h) from edge view

4 Statistical analysis of fatigue life data

The scope of the analysis was to examine the stochastic characteristics of fatigue life and statistically test the validity of the acquired data (Philippidis and Vassilopoulos, 2000).

4.1 Distribution

The log-normal distribution and the three-parameter (3P) Weibull distribution can well describe the fatigue life data of the virgin T700/MTM46 laminates at various stress levels (Feng et al., 2016). In this section, we also assume that the fatigue life data of the moisture-saturated specimens also obey the above two distributions. The relations used to define the cumulative distribution function (CDF) F are listed in the following.

Log-normal distribution is

$$F(\lg x;\mu,\sigma)=\int_{-\infty}^{\lg x}\frac{1}{\sigma\sqrt{2\pi}}\exp\left[-\frac{(\lg x-\mu)^2}{2\sigma^2}\right]\mathrm{d}(\lg x), \tag{3}$$

and 3P Weibull distribution is

$$F\left(x;\alpha,\beta,b\right)=1-\exp\left[-\left(\frac{x-\alpha}{\beta-\alpha}\right)^b\right],\quad x\geq 0, \tag{4}$$

where lg$x$ is a random variable, μ and σ represent expectation and standard deviation of the random variable, respectively, in Eq. (3). For Eq. (4), x represents a random variable, α and β are the lower limit parameter and shape parameter of the random variable, respectively, and b represents the characteristic parameter.

Generally, the empirical frequency function can be defined as

$$F\left(x_i\right)=\frac{i}{n+1}, \tag{5}$$

where n is the sample size, x_i is a random variable, and i represents the serial number of fatigue life data arranged in ascending order.

In Table 5, maximum likelihood estimate (MLE) parameters (Bury, 1999) and least square estimate (LSE) parameters (Chen et al., 2002) are listed for each set of fatigue data under different stress levels for log-normal and 3P Weibull distributions, respectively.

4.2 Statistical test

The Pearson correlation coefficient r was adopted to determine whether the fatigue life data obey log-normal distribution or 3P Weibull distribution at each stress level. The correlation coefficient r is described by (Chen, 2002)

$$r=\frac{L_{XY}}{\sqrt{L_{XX}L_{YY}}}, \tag{6}$$

where

$$L_{XX}=\sum_{i=1}^{n}(X_i-\bar{X})^2, \tag{7}$$

$$L_{YY}=\sum_{i=1}^{n}(Y_i-\bar{Y})^2, \tag{8}$$

$$L_{XY}=\sum_{i=1}^{n}(X_i-\bar{X})(Y_i-\bar{Y}), \tag{9}$$

X_i and Y_i are random variables, and $\bar{X}$ and $\bar{Y}$ are the average values of X_i and Y_i, respectively.

A good correlation between experimental data and theoretical distributions can be verified if $|r|$ is close to 1. It should be noticed that only five laminates were used in these tension–tension fatigue experiments due to the high experimental cost at each stress level. Thus, the corresponding correlation coefficient threshold value r_γ at a certain confidence level γ, needs to be determined by (Gao, 1986)

$$r_\gamma=\frac{t_\gamma(n-2)}{\sqrt{(n-2)+t_\gamma^2(n-2)}}, \tag{10}$$

where $t_\gamma(n-2)$ represents the Student distribution.

If the correlation coefficient r calculated for log-normal distribution or 3P Weibull distribution under a certain confidence level γ is larger than the threshold value r_γ, it is confirmed that there is a favorable comparison between experimental data and statistical distribution. When n=5 and γ=95%, r_γ is 0.878.

The correlation coefficients r for the aforementioned distributions are given in Table 5. From it, the fatigue life data can be modeled for these distributions for the whole range of stress levels. However, according to the value of r, the fatigue data can be described better under most stress levels as a log-normal distribution. Meanwhile, for convenience of comparison, the reliable fatigue life of saturated specimens studied later also uses a log-normal distribution, as in the study on reliable fatigue life of the virgin specimens (Feng et al., 2016).

5 Reliability analysis for fatigue life

In most fatigue experiments for CFRP materials, the number of samples is insufficient because of the high experimental cost. It is therefore necessary to discuss the reliable fatigue life at a certain reliability p and confidence level γ. In this section, the reliable fatigue life of the specimens is calculated using log-normal distribution. The method adopted in the calculation is the same as that in (Feng et al., 2016).

The log-reliable fatigue life $\hat{x}_{p,\gamma}$ under the reliability p and the confidence level γ, can be expressed as (Gao, 1986)

$$\hat{x}_{p,\gamma}=\overline{x}+\left\{\frac{\mu_p-\mu_\gamma\sqrt{\frac{1}{n}\left[1-\frac{\mu_\gamma^2}{2(n-1)}\right]+\frac{\mu_p^2}{2(n-1)}}}{1-\frac{\mu_\gamma^2}{2(n-1)}}\right\}\cdot\hat{\sigma}, \tag{11}$$

where $\overline{x}$ and n are the mean of the logarithmic fatigue life and the number of specimens, respectively. μ_p and μ_γ represent the normal distribution values corresponding to p and γ, respectively. The expression of $\hat{\sigma}$ is

$$\hat{\sigma}=\sqrt{\frac{n-1}{2}}\frac{\Gamma\left(\frac{n-1}{2}\right)}{\Gamma\left(\frac{n}{2}\right)}\cdot s_x, \tag{12}$$

where s_x is the standard deviation of the samples, and Γ is the gamma function. Therefore, under the reliability p and confidence level γ, the reliable fatigue life $N_{p,\gamma}$ can be expressed as

$$N_{p,\gamma}=10^{\hat{x}_{p,\gamma}}. \tag{13}$$

In order to compare with the fatigue reliability life of the virgin specimens in (Feng et al., 2016), the reliable fatigue life $N_{p,\gamma}$ with the reliability p=95% at various confidence levels was calculated in Table 6, and $N_{p,\gamma}$ with the confidence level γ=95% at various reliability levels was calculated in Table 7. It can be found that the reliable fatigue life $N_{p,\gamma}$ decreases with increasing reliability or confidence level at the same stress level, and $N_{p,\gamma}$ decreases with the increase of the stress level under the same reliability or confidence.

The reliable fatigue life data of virgin T700/MTM46 laminates at confidence level γ=95% at various reliability levels in (Feng et al., 2016) as well as those of moisture-saturated specimens in Table 7 are plotted in Fig. 11. It can be seen that the reliable fatigue life of the moisture-saturated specimens under the same reliability level, confidence level, and stress level decreases sharply compared with that of virgin specimens. For example, when γ=95%, the reliable fatigue life of T700/MTM46 laminates decreases by 29.7%, 34.1%, 33.8%, and 40.3% at reliabilities p of 0.50, 0.65, 0.80, and 0.95, respectively, under the q=0.75 stress level. This phenomenon is mainly due to the fatigue life data of T700/MTM46 laminates decreasing after hygrothermal aging at the same

Table 5 Fatigue life data: parameters and correlation coefficients for two statistical distributions

q	Log-normal distribution			3P Weibull distribution			
	μ	σ	r	α	β	b	r
0.90	2.8682	0.3880	0.9738	0	1178	1.0778	0.9897
0.85	3.9559	0.3796	0.9717	2124.7	13 740	0.6544	0.9390
0.80	4.6988	0.4561	0.9819	10 694	82 342	0.5516	0.9764
0.75	5.5137	0.2778	0.9780	34 782	426 050	1.6462	0.9717
0.70	5.6160	0.2127	0.9823	56 181	534 470	1.4655	0.9752
0.65	5.8795	0.1137	0.9806	192 440	815 730	2.1059	0.9789

Table 6 Reliable fatigue life data with reliability p=95% at various confidence levels

q	γ=50%		γ=65%		γ=80%		γ=95%	
	$\hat{x}_{p,\gamma}$	$N_{p,\gamma}$	$\hat{x}_{p,\gamma}$	$N_{p,\gamma}$	$\hat{x}_{p,\gamma}$	$N_{p,\gamma}$	$\hat{x}_{p,\gamma}$	$N_{p,\gamma}$
0.90	2.1917	156	2.0605	115	1.8520	71	1.1447	14
0.85	3.2941	1968	3.1657	1465	2.9618	916	2.2700	186
0.80	3.9036	8009	3.7494	5616	3.5043	3194	2.6730	471
0.75	5.0293	106 979	4.9354	86 179	4.7861	61 104	4.2797	19 040
0.70	5.2480	177 011	5.1764	150 107	5.0627	115 519	4.6768	47 506
0.65	5.6813	480 065	5.6428	439 339	5.5817	381 677	5.3744	236 803

Table 7 Reliable fatigue life data with confidence level γ=95% at various reliability levels

q	p=50%		p=65%		p=80%		p=95%	
	$\hat{x}_{p,\gamma}$	$N_{p,\gamma}$	$\hat{x}_{p,\gamma}$	$N_{p,\gamma}$	$\hat{x}_{p,\gamma}$	$N_{p,\gamma}$	$\hat{x}_{p,\gamma}$	$N_{p,\gamma}$
0.90	2.4963	314	2.2316	170	1.8647	73	1.1447	14
0.85	3.5921	3909	3.3331	2153	2.9743	942	2.2700	186
0.80	4.2617	18 268	3.9506	8925	3.5193	3306	2.6730	471
0.75	5.2474	176 767	5.0579	114 262	4.7952	62 402	4.2797	19 040
0.70	5.4142	259 537	5.2698	186 123	5.0696	117 385	4.6768	47 506
0.65	5.7706	589 658	5.6930	493 174	5.5854	384 975	5.3744	236 803

stress level, from the perspective of fatigue life data. Essentially, the main reason for the serious decline of reliable fatigue life is that damage, such as micropore and micro-delamination, has been generated in the specimens during the moisture absorption process, and then will grow and deteriorate more rapidly in the fatigue process. This can also be inferred from Fig. 11; the stiffness of the moisture-saturated specimens decreases more than that of virgin specimens at the same percentage of fatigue life. The fatigue failure mode is dominated by delamination failure. In particular, the micro-delamination generated during the moisture absorption process allows much easier expansion under the fatigue loading, which in turn leads to a serious decline in the fatigue life of the saturated specimens.

According to Eq. (1), the p-γ-S-N curve can be expressed by

$$S = \lg C_{p,\gamma} / (m_{p,\gamma} \lg \mathrm{e}) + 1 / (m_{p,\gamma} \lg \mathrm{e} \cdot \lg N_{p,\gamma}), \quad (14)$$

where $C_{p,\gamma}$ and $m_{p,\gamma}$ are material constants at the reliability p and the confidence level γ. Based on the data in Tables 6 and 7, the p-γ-S-N curves of the moisture-saturated T700/MTM46 laminates under various stress levels can be plotted by using Eq. (14). Then the p-γ-S-N surfaces where the reliable fatigue life under any reliability and confidence levels can be determined are plotted in Fig. 12. Obviously, the lower the stress level, the higher the position of the p-γ-S-N surfaces in space. The reliable fatigue life of the specimens decreases as the stress level increases.

To explain the effect of hygrothermal environment on the p-γ-S-N surfaces of T700/MTM46 laminates, the p-γ-S-N surfaces of the virgin T700/MTM46 laminates at q=0.75 and q=0.85 stress levels were also calculated using the fatigue life data in (Feng et al., 2016) and plotted in Fig. 13. In Fig. 13, it is obvious that the p-γ-S-N surface of the moisture-saturated specimens is below that of the virgin specimens under the same stress level, so the reliable fatigue life of the moisture-saturated specimens will be significantly reduced compared with that before hygrothermal aging.

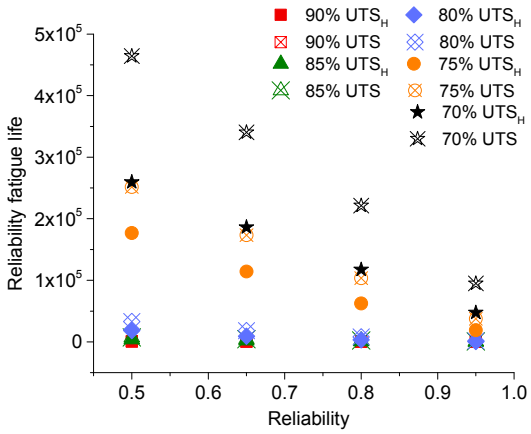

Fig. 11 Reliable fatigue life data of T700/MTM46 laminates under γ=95% (UTS_H means the UTS of moisture-saturated specimens)

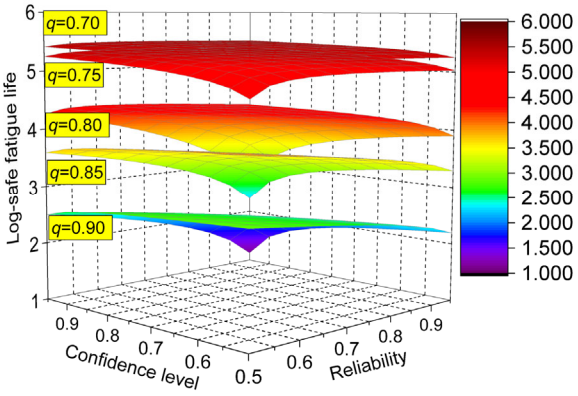

Fig. 12 p-γ-S-N surface of T700/MTM46 laminates after hygrothermal aging

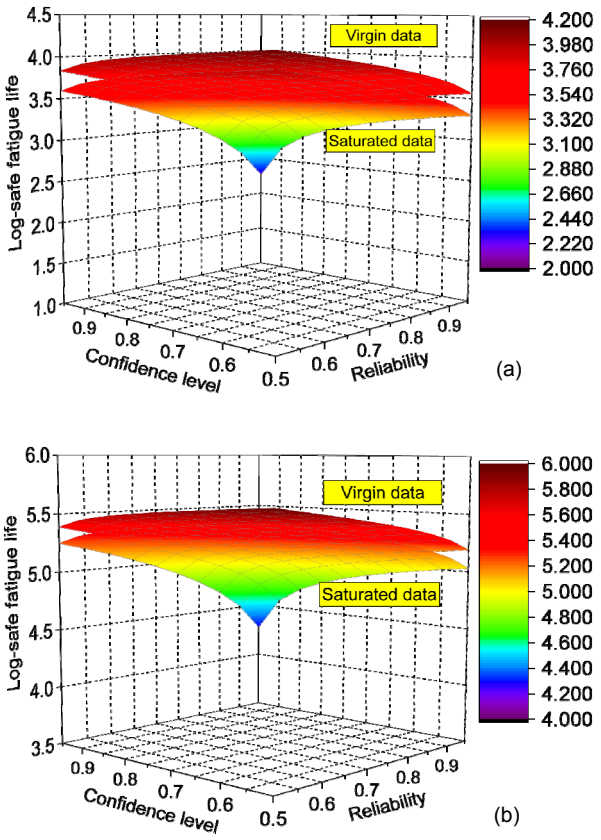

Fig. 13 ***p*-*γ*-*S*-*N* surfaces of saturated and virgin T700/MTM46 laminates**
(a) q=0.85; (b) q=0.75

6 Conclusions

Moisture absorption experiments, static tension and tension–tension fatigue experiments after hygrothermal aging on T700/MTM46 composite laminates were conducted. Particular attention was given to hygrothermal aging damage, fatigue life, stiffness degradation, damage initiation and evolution, and reliable fatigue life. The static tension and tension–tension fatigue performance of the moisture-saturated laminates were also compared with those of the virgin specimens in (Feng et al., 2016) to investigate the effects of hygrothermal environments on the performance of T700/MTM46 composite laminates. The major results and conclusions are summarized as follows:

1. The average moisture content of T700/MTM46 composite laminates was about 1.69% when effective moisture equilibrium was achieved. In the process of moisture absorption, damage such as micropore and micro-delamination appeared, but these were much less than those generated during the fatigue process. The rate of moisture absorption and damage growth during the moisture absorption process can be divided into two stages, with a rapid stage during the first 20 d and a slower stage thereafter.

2. The average static strength of specimens decreased by 1.3%, but the average values of stiffness and strain were not changed after hygrothermal aging. The stress-strain curve also increased linearly throughout the loading range. Thus, the hygrothermal environments have no significant effect on the static tensile properties of T700/MTM46 laminates. Moreover, the static failure modes of the moisture-saturated specimens were slightly different from those of the virgin specimens. There tended to be multiple fractures throughout the whole gauge length, and secondly, a slight delamination in the static failure mode.

3. The normalized stiffness degradation curves of the moisture-saturated specimens can also be divided into two distinct stages, including the steady decline stage and the rapid decline stage, similar to those of the virgin specimens. After hygrothermal aging, the stiffness at the moment before the fatigue failure of specimens was reduced by 23.5%, 22.1%, 18.2%, 17.3%, 16.9%, and 14.6% at the stress levels of q=0.65, 0.70, 0.75, 0.80, 0.85, and 0.90, respectively.

4. The fatigue limit of T700/MTM46 composite laminates after hygrothermal aging was about q=0.654, a decrease of about 6%. At the same stress level, the scattering of the fatigue life data of specimens increased after hygrothermal treatment, because the physical and chemical changes in the moisture absorption process exacerbate the non-homogeneity of the material. The damage modes of the moisture-saturated specimens during fatigue were similar to those of the virgin specimens, and the most obvious mode remains severe delamination throughout the whole gauge length. However, a certain degree of damage was generated in moisture-saturated specimens during the moisture absorption process, such as micropore and micro-delamination, which contributed to the rapidly increasing damage during fatigue. Thus, under the same fatigue cycling to life ratio, the damage of the moisture-saturated specimens was much greater than that of the virgin specimens.

5. The log-normal distribution was a better description of the fatigue life data of the moisture-saturated T700/MTM46 laminates at various stress levels. Under the assumption that it obeys a log-normal distribution, the reliable fatigue life at the same stress level decreased with increasing confidence level or reliability. The *p*-*γ*-*S*-*N* surfaces were established to predict the reliable fatigue life of the T700/MTM46 laminates. The *p*-*γ*-*S*-*N* surfaces of the moisture-saturated specimens were located under those of the virgin specimens, and the reliable fatigue life of the moisture-saturated specimens was much lower than that of the virgin specimens under the same conditions (stress level, confidence, and reliability).

Contributors

Bin-lin MA wrote the first draft of the manuscript. Yu FENG revised and edited the final version. Yu-ting HE managed the execution of research activity. Teng ZHANG, Sheng ZHANG, and Tian-yu ZHANG assisted in the experiments.

Conflict of interest

Bin-lin MA, Yu FENG, Yu-ting HE, Teng ZHANG, Sheng ZHANG, and Tian-yu ZHANG declare that they have no conflict of interest.

References

Adda-Bedia EA, Bouazza M, Tounsi A, et al., 2008. Prediction of stiffness degradation in hygrothermal aged $[\theta_m/90_n]_s$ composite laminates with transverse cracking. *Journal of Materials Processing Technology*, 199(1-3):199-205. https://doi.org/10.1016/j.jmatprotec.2007.08.002

Amara KH, Tounsi A, Benzair A, 2005. Transverse cracking and elastic properties reduction in hygrothermal aged cross-ply laminates. *Materials Science and Engineering: A*, 396(1-2):369-375. https://doi.org/10.1016/j.msea.2005.02.006

Arani AG, Zamani MH, 2018. Bending analysis of agglomerated carbon nanotube-reinforced beam resting on two parameters modified Vlasov model foundation. *Indian Journal of Physics*, 92(6):767-777. https://doi.org/10.1007/s12648-018-1162-z

ASTM (American Society for Testing and Materials), 2004. Standard Test Method for Moisture Absorption Properties and Equilibrium Conditioning of Polymer Matrix Composite Materials, ASTM D5229/D5229M-92(2004). National Standards of USA.

ASTM (American Society for Testing and Materials), 2007. Standard Test Method for Tensile Properties of Polymer Matrix Composite Materials, ASTM D3039/D3039M-07. National Standards of USA.

ASTM (American Society for Testing and Materials), 2012. Standard Test Method for Tension-tension Fatigue of Polymer Matrix Composite Materials, ASTM D3479/D3479M-2012. National Standards of USA.

Bao LR, Yee AF, 2002. Effect of temperature on moisture absorption in a bismaleimide resin and its carbon fiber composites. *Polymer*, 43(14):3987-3997. https://doi.org/10.1016/S0032-3861(02)00189-1

Bury K, 1999. Statistical Distributions in Engineering. Cambridge University Press, Cambridge, UK.

Caminero MA, García-Moreno I, Rodríguez GP, 2018. Experimental study of the influence of thickness and ply-stacking sequence on the compression after impact strength of carbon fibre reinforced epoxy laminates. *Polymer Testing*, 66:360-370. https://doi.org/10.1016/j.polymertesting.2018.02.009

Chen CY, 2002. Fatigue and Fracture. Huazhong Science and Technology University Press, Wuhan, China (in Chinese).

Chen YL, Yang XH, Qin HQ, 2002. Study on corrosion damage distribution law of aircraft structure. *Materials Science & Engineering*, 20(3):378-380 (in Chinese). https://doi.org/10.3969/j.issn.1673-2812.2002.03.018

Degenhardt R, Kling A, Rohwer K, et al., 2008. Design and analysis of stiffened composite panels including post-buckling and collapse. *Computers & Structures*, 86(9):919-929. https://doi.org/10.1016/j.compstruc.2007.04.022

Degenhardt R, Zimmermann R, Kling A, et al., 2014. New robust design guideline for imperfection sensitive composite launcher structures. Proceedings of the 13th European Conference on Spacecraft Structures.

Duan X, Yao WX, 2002. Multi-directional stiffness degradation induced by matrix cracking in composite laminates. *International Journal of Fatigue*, 24(2-4):119-125. https://doi.org/10.1016/S0142-1123(01)00066-4

Feng Q, Li M, Gu YZ, et al., 2010. Experimental research on hygrothermal properties of carbon fiber/epoxy resin composite under different hygrothermal conditions. *Acta Materiae Compositae Sinica*, 27(6):16-20 (in Chinese). https://doi.org/10.13801/j.cnki.fhclxb.2010.06.030

Feng Y, He YT, An T, et al., 2015. Effect of hygrothermal condition on buckling and post-buckling performance of CCF300/5228A aero composite stiffened panel under axial compression. *Journal of Reinforced Plastics and Composites*, 34(12):989-999. https://doi.org/10.1177/0731684415585381

Feng Y, Gao C, He YT, et al., 2016. Investigation on tension–tension fatigue performances and reliability fatigue life of T700/MTM46 composite laminates. *Composite Structures*, 136:64-74. https://doi.org/10.1016/j.compstruct.2015.09.057

Feng Y, He YT, Zhang HY, et al., 2017a. Effect of fatigue loading on impact damage and buckling/post-buckling

behaviors of stiffened composite panels under axial compression. *Composite Structures*, 164:248-262. https://doi.org/10.1016/j.compstruct.2016.12.069

Feng Y, He YT, Tan XF, et al., 2017b. Experimental investigation on different positional impact damages and shear-after-impact (SAI) behaviors of stiffened composite panels. *Composite Structures*, 178:232-245. https://doi.org/10.1016/j.compstruct.2017.06.053

Feng Y, He YT, Tan XF, et al., 2017c. Investigation on impact damage evolution under fatigue load and shear-after-impact-fatigue (SAIF) behaviors of stiffened composite panels. *International Journal of Fatigue*, 100:308-321. https://doi.org/10.1016/j.ijfatigue.2017.03.046

Gao C, He Y, Zhang H, 2013. Performance deregulation rule of aircraft fatigue critical components in consideration of calendar environment. Proceedings of the 13th International Conference on Fracture, p.1-8.

Gao ZT, 1986. Fatigue Applied Statistics. National Defence Industry Press, Beijing, China (in Chinese).

García-Moreno I, Caminero MÁ, Rodriguez GP, et al., 2019a. Effect of thermal ageing on the impact and flexural damage behaviour of carbon fibre-reinforced epoxy laminates. *Polymers*, 11(1):80. https://doi.org/10.3390/polym11010080

García-Moreno I, Caminero MÁ, Rodríguez GP, et al., 2019b. Effect of thermal ageing on the impact damage resistance and tolerance of carbon-fibre-reinforced epoxy laminates. *Polymers*, 11(1):160. https://doi.org/10.3390/polym11010160

Giancane S, Panella FW, Dattoma V, 2010. Characterization of fatigue damage in long fiber epoxy composite laminates. *International Journal of Fatigue*, 32(1):46-53. https://doi.org/10.1016/j.ijfatigue.2009.02.024

Gibson RF, 2016. Principles of Composite Material Mechanics. CRC Press, Boca Raton, New York, USA.

Hosoi A, Kawada H, Yoshino H, 2006. Fatigue characteristics of quasi-isotropic CFRP laminates subjected to variable amplitude cyclic two-stage loading. *International Journal of Fatigue*, 28(10):1284-1289. https://doi.org/10.1016/j.ijfatigue.2006.02.039

Joshi OK, 1983. The effect of moisture on the shear properties of carbon fibre composites. *Composites*, 14(3):196-200. https://doi.org/10.1016/0010-4361(83)90005-8

Judawisastra H, Ivens J, Verpoest I, 1998. The fatigue behaviour and damage development of 3D woven sandwich composites. *Composite Structures*, 43(1):35-45. https://doi.org/10.1016/S0263-8223(98)00093-2

Karbhari VM, Xian GJ, 2009. Hygrothermal effects on high V_F pultruded unidirectional carbon/epoxy composites: moisture uptake. *Composites Part B: Engineering*, 40(1):41-49. https://doi.org/10.1016/j.compositesb.2008.07.003

Khechen A, 2015. Study of Adhesively Bonded Repairs in Aircraft CFRP Primary Structures. MS Thesis, Laval University, Québec, Canada.

Kootsookos A, Mouritz AP, 2004. Seawater durability of glass- and carbon-polymer composites. *Composites Science and Technology*, 64(10-11):1503-1511. https://doi.org/10.1016/j.compscitech.2003.10.019

Mallela UK, Upadhyay A, 2016. Buckling load prediction of laminated composite stiffened panels subjected to in-plane shear using artificial neural networks. *Thin-Walled Structures*, 102:158-164. https://doi.org/10.1016/j.tws.2016.01.025

Manjunatha CM, Taylor AC, Kinloch AJ, et al., 2010. The tensile fatigue behaviour of a silica nanoparticle-modified glass fibre reinforced epoxy composite. *Composites Science and Technology*, 70(1):193-199. https://doi.org/10.1016/j.compscitech.2009.10.012

Maria M, 2013. Advanced composite materials of the future in aerospace industry. *Incas Bulletin*, 5(3):139-150. https://doi.org/10.13111/2066-8201.2013.5.3.14

Mohaghegh M, 2018. University of Washington/Boeing certificate programs in aircraft structures and composite materials. AIAA/ASCE/AHS/ASC Structures, Structural Dynamics, and Materials Conference, p.2252.

Montesano J, Fawaz Z, Behdinan K, et al., 2012. Fatigue damage in on-axis and off-axis woven-fiber/resin composite. *Key Engineering Materials*, 488:230-233.

Montesano J, Fawaz Z, Bougherara H, 2013. Characterization of Fatigue Loaded Carbon Fiber Reinforced Polymer Matrix Composites Using Infrared Thermography. Sciences and Techniques Organization-OTAN, Toronto, Canada.

Montesano J, McCleave B, Singh CV, 2018. Prediction of ply crack evolution and stiffness degradation in multidirectional symmetric laminates under multiaxial stress states. *Composites Part B: Engineering*, 133:53-67. https://doi.org/10.1016/j.compositesb.2017.09.016

Patel SR, Case SW, 2000. Durability of a graphite/epoxy woven composite under combined hygrothermal conditions. *International Journal of Fatigue*, 22(9):809-820. https://doi.org/10.1016/S0142-1123(00)00041-4

Peng TS, Liu YM, Saxena A, et al., 2015. In-situ fatigue life prognosis for composite laminates based on stiffness degradation. *Composite Structures*, 132:155-165. https://doi.org/10.1016/j.compstruct.2015.05.006

Philippidis TP, Vassilopoulos AP, 2000. Fatigue design allowables for GRP laminates based on stiffness degradation measurements. *Composites Science and Technology*, 60(15):2819-2828. https://doi.org/10.1016/S0266-3538(00)00150-0

Riccio A, 2015. Damage Growth in Aerospace Composites. Springer, Cham, Switzerland. https://doi.org/10.1007/978-3-319-04004-2

Riccio A, di Felice G, Saputo S, et al., 2013. A numerical study on low velocity impact induced damage in stiffened composite panels. *Journal of Computational Simulation*

and Modeling, 3(1):44-47.

Riccio A, Raimondo A, Fragale S, et al., 2014. Delamination buckling and growth phenomena in stiffened composite panels under compression. Part I: an experimental study. *Journal of Composite Materials*, 48(23):2843-2855. https://doi.org/10.1177/0021998313502741

Sun P, Zhao Y, Luo YF, et al., 2011. Effect of temperature and cyclic hygrothermal aging on the interlaminar shear strength of carbon fiber/bismaleimide (BMI) composite. *Materials & Design*, 32(8-9):4341-4347. https://doi.org/10.1016/j.matdes.2011.04.007

Tate JS, Kelkar AD, 2008. Stiffness degradation model for biaxial braided composites under fatigue loading. *Composites Part B: Engineering*, 39(3):548-555. https://doi.org/10.1016/j.compositesb.2007.03.001

Tual N, Carrere N, Davies P, et al., 2015. Characterization of sea water ageing effects on mechanical properties of carbon/epoxy composites for tidal turbine blades. *Composites Part A: Applied Science and Manufacturing*, 78: 380-389. https://doi.org/10.1016/j.compositesa.2015.08.035

van Paepegem W, Degrieck J, 2002. A new coupled approach of residual stiffness and strength for fatigue of fibre-reinforced composites. *International Journal of Fatigue*, 24(7):747-762. https://doi.org/10.1016/S0142-1123(01)00194-3

Yao WX, Himmel N, 1999. Statistical analysis of data from truncated fatigue life and corresponding residual strength experiments for polymer matrix composites. *International Journal of Fatigue*, 21(6):581-585. https://doi.org/10.1016/S0142-1123(99)00005-5

Zafar A, Bertocco F, Schjødt-Thomsen J, et al., 2012. Investigation of the long term effects of moisture on carbon fibre and epoxy matrix composites. *Composites Science and Technology*, 72(6):656-666. https://doi.org/10.1016/j.compscitech.2012.01.010

Zhang LJ, Zhao Y, Luo YF, et al., 2012. On the interfacial properties of CCF300/QY8911 composite with cyclical hygrothermal treatments. *Journal of Materials Engineering*, (2):25-29 (in Chinese). https://doi.org/10.3969/j.issn.1001-4381.2012.02.007

Zhao X, Wang X, Wu ZS, et al., 2016. Fatigue behavior and failure mechanism of basalt FRP composites under long-term cyclic loads. *International Journal of Fatigue*, 88: 58-67. https://doi.org/10.1016/j.ijfatigue.2016.03.004

中文概要

题　目：湿热环境对 T700/MTM46 复合材料层合板拉-拉疲劳性能和疲劳可靠寿命的影响

目　的：碳纤维复合材料的疲劳特性对航空结构的安全性和可靠性有很大的影响，而湿热环境对复合材料性能的退化作用较大。本文针对湿热环境对碳纤维复合材料层合板的拉-拉疲劳性能和疲劳可靠寿命的影响进行研究，为碳纤维复合材料在实际湿热环境中的应用提供参考。

创新点：1. 通过实验分析得到碳纤维复合材料层合板在吸湿过程中的损伤演化过程；2. 采用实验和理论分析的方法，研究湿热环境对碳纤维复合材料层合板拉-拉疲劳性能和疲劳可靠寿命的影响。

方　法：1. 通过吸湿实验，观测分析得到碳纤维复合材料层合板在湿热老化过程中的损伤演化过程；2. 通过疲劳试验，研究湿热环境下碳纤维复合材料的疲劳损伤演化过程、刚度退化规律和损伤失效模式；3. 通过理论分析，采用疲劳可靠寿命预测模型，得到湿热环境下碳纤维复合材料的疲劳可靠寿命。

结　论：1. T700/MTM46 复合材料层合板在吸湿过程中，出现了微孔和微脱层等损伤，但比疲劳过程中产生的损伤要小得多；2. 与常温环境相比，湿热环境下实验件的刚度退化曲线的变化趋势保持一致，但刚度下降幅度增大；3. 与常温环境相比，湿热环境下实验件的疲劳极限降低约 6%，疲劳损伤模式相似，但在相同疲劳循环数下的损伤程度加剧；4. 在湿热环境作用下，实验件的疲劳可靠寿命大大降低。

关键词：碳纤维复合材料；湿热环境；疲劳性能；损伤演化；*p*-*γ*-*S*-*N* 曲面